Pitch angle scattering of relativistic electrons near electromagnetic ion cyclotron resonances in diverging magnetic fields

B Eliasson[1,2] and K Papadopoulos[2]

[1] SUPA, Physics Department, University of Strathclyde, Glasgow, Scotland, United Kingdom
[2] Departments of Physics and Astronomy, University of Maryland, College Park, Maryland, United States of America

E-mail: bengt.eliasson@strath.ac.uk

CrossMark

Abstract

A theoretical study of the propagation of left-hand polarized shear Alfvén waves in spatially decreasing magnetic field geometries near the EMIC resonance, including the spectrum and amplitude of the mode converted EMIC waves and the pitch angle scattering of relativistic electrons transiting the resonant region, is presented. The objective of the paper is to motivate an experimental study of the subject using the UCLA LAPD chamber. The results are relevant in exploring the possibility that shear Alfvén waves strategically injected into the radiation belts using either ionospheric heating from ground based RF transmitters or injected by transmitters based on space platforms can enhance the precipitation rate of trapped relativistic electrons. Effects of multi-ionic composition are also investigated.

(Some figures may appear in colour only in the online journal)

1. Introduction

Electromagnetic ion cyclotron (EMIC) waves are left-hand polarized shear Alfvén waves propagating parallel to the ambient magnetic field with frequency approaching the ion cyclotron frequency. They are often found in the radiation belts and are considered primary candidates for precipitation of MeV electrons trapped in the belts. The surprising strength of the interaction of waves with frequency ω much smaller than the electron cyclotron frequency ω_{ce} ($\omega \ll \omega_{ce}$) with relativistic electrons can be appreciated by referring to the dispersion relation of low frequency waves propagating parallel to the ambient magnetic field B_z in multispecies plasma,

given by

$$\frac{k_z^2 c^2}{\omega^2} = 1 - \sum_j \frac{\omega_{pj}^2}{\omega(\omega - \omega_{cj})} - \frac{\omega_{pe}^2}{\omega(\omega + \omega_{ce})}, \quad (1)$$

where $\omega_{pj} = \sqrt{n_{j0}q_j^2/\varepsilon_0 m_j}$ and $\omega_{cj} = q_j B/m_j$ are the ion plasma and cyclotron frequencies, respectively, of ion species j, and $\omega_{pe} = \sqrt{n_0 e^2/\varepsilon_0 m_e}$ and $\omega_{ce} = eB/m_e$ are the electron plasma and cyclotron frequencies. (The other symbols have their usual meaning.)

Figure 1 shows an example of this dispersion relation for a plasma with a mixture of hydrogen, helium and oxygen ions such as encountered in the radiation belts. Notice that

$$\frac{k_z^2 c^2}{\omega^2} \to \infty \text{ for } \omega \to \omega_{cj}. \quad (2)$$

As a result there will be a wavenumber range close to the ion resonance where electrons with energy $\gamma m_e c^2$ will satisfy the anomalous cyclotron resonance condition for pitch angle
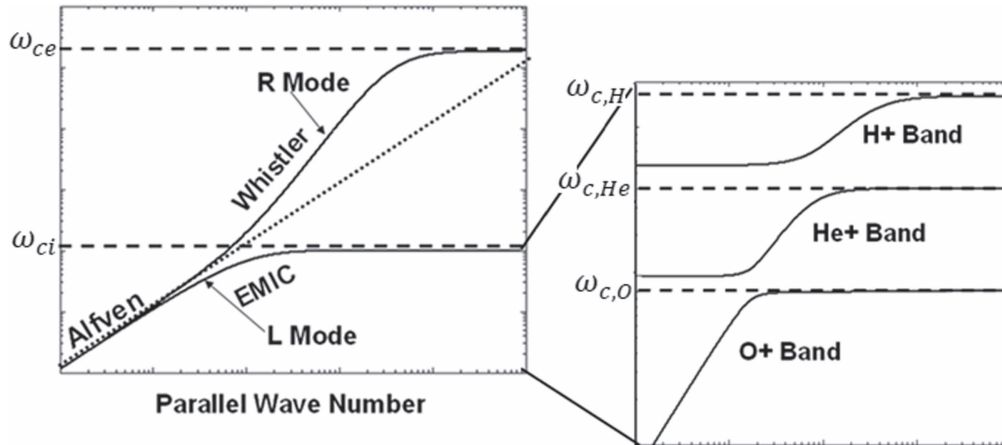
Figure 1. EMIC dispersion relation for a multi-ionic plasma including hydrogen (H), helium (He) and oxygen (O) ions.

scattering

$$\omega - k_z v_z = -\frac{\omega_{ce}}{\gamma}. \tag{3}$$

Since $\omega \ll \omega_{ce}$, the condition given by equation (3) reduces to a wavelength condition given by

$$\frac{1}{k_z} \approx \frac{\gamma v_z}{\omega_{ce}}. \tag{4}$$

In most of previous work on the subject it was assumed that the EMIC waves are excited by unstable distributions of ring current ions both inside and outside the plasmapause and propagate in regions localized in longitude. The electrons drifting eastward in the Earth's magnetic field encounter the localized waves and are scattered in pitch angle with scattering rate that depends critically on the wave amplitude, frequency and chirping rate of the EMIC waves (Summers *et al* 2007, Omura *et al* 2010, Morley *et al* 2010, Engebretson *et al* 2015, Kubota *et al* 2015). In this paper we want to propose that EMIC waves with controlled bandwidth and chirping rate can be generated by mode conversion of shear Alfvén waves propagating along the magnetic field lines when they encounter the EMIC cyclotron resonance. Such a possibility was addressed recently by Shao *et al* (2009) who proposed shear Alfvén waves generated by ionospheric heating can create regions of strong EMIC waves when they encounter the O$^+$ cyclotron resonance at altitude between 1000 and 2000 km. Alternatively such waves can be artificially injected at the appropriate regions from space-based transmitters. The underlying mode conversion physics parallels the 'magnetic beach' experiments and theory conducted by, among others, Stix (1958), Stix and Palladino (1958), and Roberts and Hershkowitz (1992), and occurs when a left-hand polarized shear Alfvén wave propagates parallel to a weakening magnetic field.

The objective of this paper is to motivate a laboratory experiment to study mode conversion of shear Alfvén waves in a mirror geometry, such as it occurs in the radiation belts, and determine the pitch angle scattering rate of energetic electrons interacting with the waves through the anomalous cyclotron resonance interaction by controlling the parameters

of the injected shear Alfvén waves. Such an experiment can ideally be conducted at the UCLA LAPD device that has already been the site of numerous experimental studies of kinetic shear Alfvén waves with multispecies ion plasmas in mirror geometries (Vincena *et al* 2001, 2010, 2011, 2013, Farmer and Morales 2013). These studies focused on the kinetic Alfvén wave injection and the resultant ion heating and ion–ion hybrid resonant effects. It should be noted that pitch angle scattering of energetic electrons have been studied using whistler waves (Van Compernolle *et al* 2014) and Alfvén waves (Wang *et al* 2012, 2014).

In this paper we investigate the wave propagation of EMIC waves near cyclotron resonances, including the resultant wave spectra near the singularity and the pitch angle scattering of relativistic electrons injected in the turbulent region. The linear Hall-MHD model with an inhomogeneous magnetic field is presented in section 2, where analytic solutions (Stix 1960, 1992) of the waveform near cyclotron resonances are discussed for waves propagating parallel to the magnetic field. The analytic results are compared to numerical simulations in section 3. In section 4, the analytic solution for the wave magnetic field is used to derive the pitch angle diffusion coefficient and compute the scattering of relativistic electrons for typical UCLA LAPD parameters. Finally, conclusions are drawn in section 5.

2. Mathematical model

To study the propagation of EMIC waves in spatially varying plasma, we use the cold Hall-MHD model involving the linearized ion momentum equation for ion species j with charge q_j and mass m_j,

$$\frac{\partial \mathbf{v}_j}{\partial t} = \frac{q_j}{m_j}(\mathbf{E} + \mathbf{v}_j \times \mathbf{B}_0) - \nu_j \mathbf{v}_j, \tag{5}$$

and the electron momentum equation for the inertialess electrons

$$-e(\mathbf{E} + \mathbf{v}_e \times \mathbf{B}_0) - m_e \nu_e \mathbf{v}_e = 0, \tag{6}$$

where ν_j and ν_e are ion and electron damping rates due to collisions. The equations of motion are coupled with

Ampère's and Faraday's laws,

$$\nabla \times \mathbf{B} = \mu_0 \left(\sum_j q_j n_{j0} \mathbf{v}_j - en_0 \mathbf{v}_e \right), \qquad (7)$$

and

$$\frac{\partial \mathbf{B}}{\partial t} = -\nabla \times \mathbf{E}, \qquad (8)$$

respectively, and where quasineutrality requires that $\sum_j q_j n_{j0} = en_0$ where n_0 is the electron number density.

2.1. Propagation parallel to the magnetic field

As the EMIC wave approaches a cyclotron resonance, its parallel wave vector component gradually increases. For an L-polarized wave with frequency ω propagating parallel to $\mathbf{B}_0 = B_0 \hat{\mathbf{z}}$, such that $\mathbf{E} = \mathrm{Re}[E(z)(\hat{\mathbf{x}} - i\hat{\mathbf{y}})e^{-i\omega t}]$ and similarly for $\mathbf{v}_j$, $\mathbf{v}_e$ and $\mathbf{B}$, equations (5)–(8) turn into scalar complex valued equations for the envelopes,

$$-i\omega v_j = \frac{q_j}{m_j}(E - iv_j B_0) - \nu_j v_j, \qquad (9)$$

$$-e(E - iv_e B_0) - m_e \nu_e v_e = 0, \qquad (10)$$

$$i\frac{\partial B}{\partial z} = \mu_0 \left(\sum_j q_j n_{j0} v_j - en_0 v_e \right), \qquad (11)$$

and

$$-i\omega B = -i\frac{\partial E}{\partial z}, \qquad (12)$$

respectively. Eliminating v_j, v_e and B from equations (9)–(12), the equation for the electric field envelope for can be written

$$\frac{\partial^2 E}{\partial z^2} = \frac{1}{c^2} \left(\sum_j \frac{\omega \omega_{pj}^2}{\omega - \omega_{cj} + i\nu_j} + \frac{\omega \omega_{pe}^2}{\omega_{ce} + i\nu_e} \right) E. \qquad (13)$$

The cyclotron and plasma frequencies vary in space depending on the profiles of the number densities and the magnetic field. In the absence of collisions, resonances occur where $\omega = \omega_{cj}$ so that the expression in parenthesis on the right-hand side of equation (13) diverges, while ion–ion hybrid cutoffs occur when this expression vanishes, introducing stop bands between the ion cyclotron resonances (e.g. Perkins 1977, Summers and Thorne 2003). In an inhomogeneous magnetic field, the ion–ion hybrid cutoffs represent reflecting layers for EMIC waves as they propagate towards converging magnetic fields and their wavelengths increase, while the ion cyclotron resonances represent absorbing layers, where the EMIC wavelength decreases and the wave energy is converted to kinetic energy of the ions. The EMIC waves are expected to pitch angle scatter electrons most efficiently near the short-wavelength EMIC resonances where the resonance condition (4) can be fulfilled, while the ion–ion resonance cutoffs occur at long wavelengths with no efficient electron pitch angle scattering.

2.2. Analytic solutions near resonance

To obtain analytic solutions of the wave profiles near cyclotron resonances, we assume a diverging ambient magnetic field decreasing with z. Near the location of the ion cyclotron resonance, $z = z_0$, where $\omega = \omega_{cj}$, we can expand $\omega_{cj} \approx \omega(1 - \xi/L)$ for $\xi/L \ll 1$, where $\xi = z - z_0$, and L is the length-scale of the decreasing magnetic field. Neglecting collisions, we then have from equation (13)

$$\frac{\partial^2 E}{\partial \xi^2} = \frac{\kappa_j}{\xi} E, \qquad (14)$$

where $\kappa_j = \omega_{pj}^2 L / c^2$. We note that E is oscillatory in space for $\xi < 0$ and evanescent for $\xi > 0$. The spatial profile of the wave near resonance depends only on the local length-scale of the magnetic field and the ion plasma frequency, and hence on the number density of the resonant ion species. The WKB approximation can be used in a slowly inhomogeneous plasma, but it breaks down close to resonances, where the plasma dielectric function varies more rapidly than the local wave vector (Stix 1960, 1992). The WKB solution would predict a highly oscillatory solution with infinitely many wavelengths near the resonance, which is generally not the case.

We next for simplicity assume that κ_j is constant. The electric field for an incoming wave propagating in the positive z direction, is given by the solution of equation (14) as (Stix 1960, 1992)

$$E = E_0 \sqrt{|\kappa_j \xi|}$$
$$\times \begin{cases} J_1(2|\kappa_j \xi|^{1/2}) - i Y_1(2|\kappa_j \xi|^{1/2}), \; \xi < 0 \\ \frac{2i}{\pi} K_1[2(\kappa_j \xi)^{1/2}], \; \xi > 0, \end{cases} \qquad (15)$$

where J_n and Y_n are Bessel functions of the first and second kind, and K_n is the modified Bessel function of second kind, of order n. The wave magnetic field is obtained from Faraday's law (12) as

$$B = \frac{1}{\omega}\frac{\partial E}{\partial z}$$
$$= B_{01} \begin{cases} J_0(2|\kappa_j \xi|^{1/2}) - i Y_0(2|\kappa_j \xi|^{1/2}), \; \xi < 0 \\ \frac{2i}{\pi} K_0[2(\kappa_j \xi)^{1/2}], \; \xi > 0, \end{cases} \qquad (16)$$

where we denoted $B_{01} = -\kappa_j E_{01}/\omega$. The ion quivering velocity is obtained from the ion momentum equation (9) as

$$v_j = \frac{iq_j/m_j}{\omega - \omega_{cj}} E \qquad (17)$$

which, using $\omega_{cj} \approx \omega(1 - \xi/L)$, gives

$$v_j = \frac{v_{j01}}{\sqrt{|\kappa_j \xi|}}$$
$$\times \begin{cases} -J_1(2|\kappa_j \xi|^{1/2}) + iY_1(2|\kappa_j \xi|^{1/2}), \; \xi < 0 \\ \frac{2i}{\pi} K_1[2(\kappa_j \xi)^{1/2}], \; \xi > 0, \end{cases} \qquad (18)$$

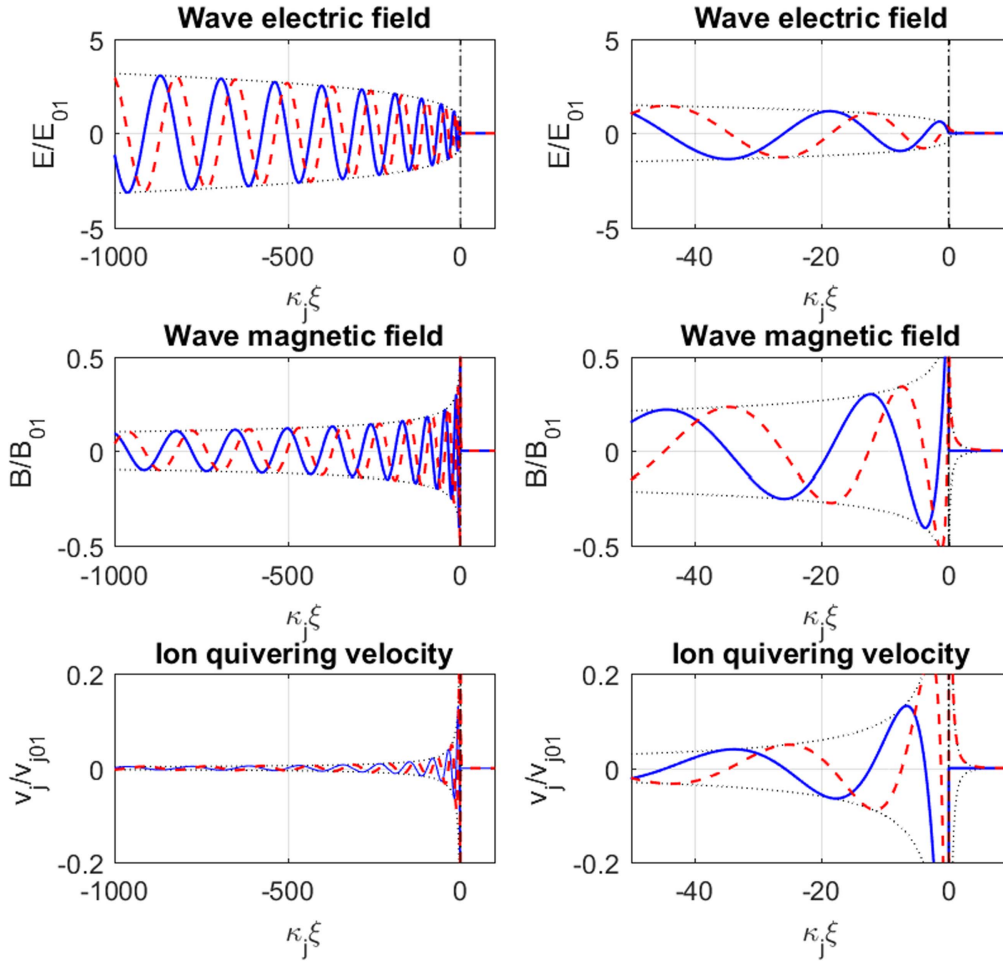with $v_{j01} = iq_j \kappa_j L E_{01}/(\omega m_j)$.

3

Figure 2. The electric field, magnetic field, and ion quivering velocity (top to bottom panels), showing real parts (blue solid lines) and imaginary parts (red dashed lines) near the resonance layer at $\xi = 0$ for a linearly decreasing magnetic field. The right-hand column shows a close-up near the resonance. The EMIC wave is evanescent and the amplitude decreases exponentially with distance for $\xi > 0$.

Figure 2 shows the spatial profiles of E, B and v_j. As noted by Stix (1960, 1992) there is a decrease of E near resonance, but the electric field remains finite, $E = iE_0/\pi$ at $\xi = 0$. For the wave magnetic field, there is a logarithmic divergence of the amplitude near $\xi = 0$. The ion quivering velocity v_j has a $1/\xi$ singularity near the resonance, implying that most of the wave energy density near the resonance is in the kinetic energy density $n_{j0}m_j v_j^2/2$ of the ions. Thus, in general the EMIC wave propagates towards the resonance where it absorbed by the acceleration of ions. It should be noted that dissipative effects such as collisions and ion cyclotron damping (and possibly nonlinear effects) will prevent infinite amplitudes at the resonance. In the derivation of the analytic solutions (Stix 1960, 1992), a small damping was kept as a mathematical tool making ξ complex valued, to avoid the singularity at the resonance.

3. Simulations of EMIC wave propagation

To assess the analytic solution for the wave magnetic field, we carry out simulations of EMIC propagation in laboratory plasma. Some details of the numerical two-ion model is given in appendix A. We use plasma parameters and dimensions relevant for the UCLA LAPD device. Figure 3 shows the propagation of EMIC waves in single ion species plasmas with a decreasing magnetic field along the z-axis (see figure 3(a)), using singly charged neon (Ne) and helium (He) ions with a homogeneous plasma density of 1.5×10^{18} m^{-3} (see figure 3(b)). To study the wave propagation near resonance in the Ne plasma, an L-polarized wave is excited at $z = 1$ m, with frequency $\omega = 4.77 \times 10^5$ s^{-1} ($f = 76$ kHz) which equals $\omega_{c,\mathrm{Ne}}$ at $B = 0.1$ T (figure 3(c)). In the He plasma, a wave with frequency $\omega = 4.82 \times 10^6$ s^{-1} ($f = 383$ kHz) is launched, which also equals $\omega_{c,\mathrm{He}}$ at $B = 0.1$ T (figure 3(d)). The EMIC wave in both cases approaches the resonance layer $z = 13$ m (indicated with red dashed lines) where the local magnetic field has decreased to 0.1 T, and only weak excitations are seen beyond the resonant layer. The local magnetic field length-scale $L = B_0(z)/|\mathrm{d}B_0/\mathrm{d}z| \approx 21$ m at the resonance layer, and the ion plasma frequencies $\omega_{p,\mathrm{Ne}} = 3.60 \times 10^8$ s^{-1} and $\omega_{p,\mathrm{He}} = 8.09 \times 10^8$ s^{-1} give $\kappa_{\mathrm{Ne}} = 30$ m^{-1} and $\kappa_{\mathrm{He}} = 153$ m^{-1} reflecting the more rapid spatial oscillations near the He
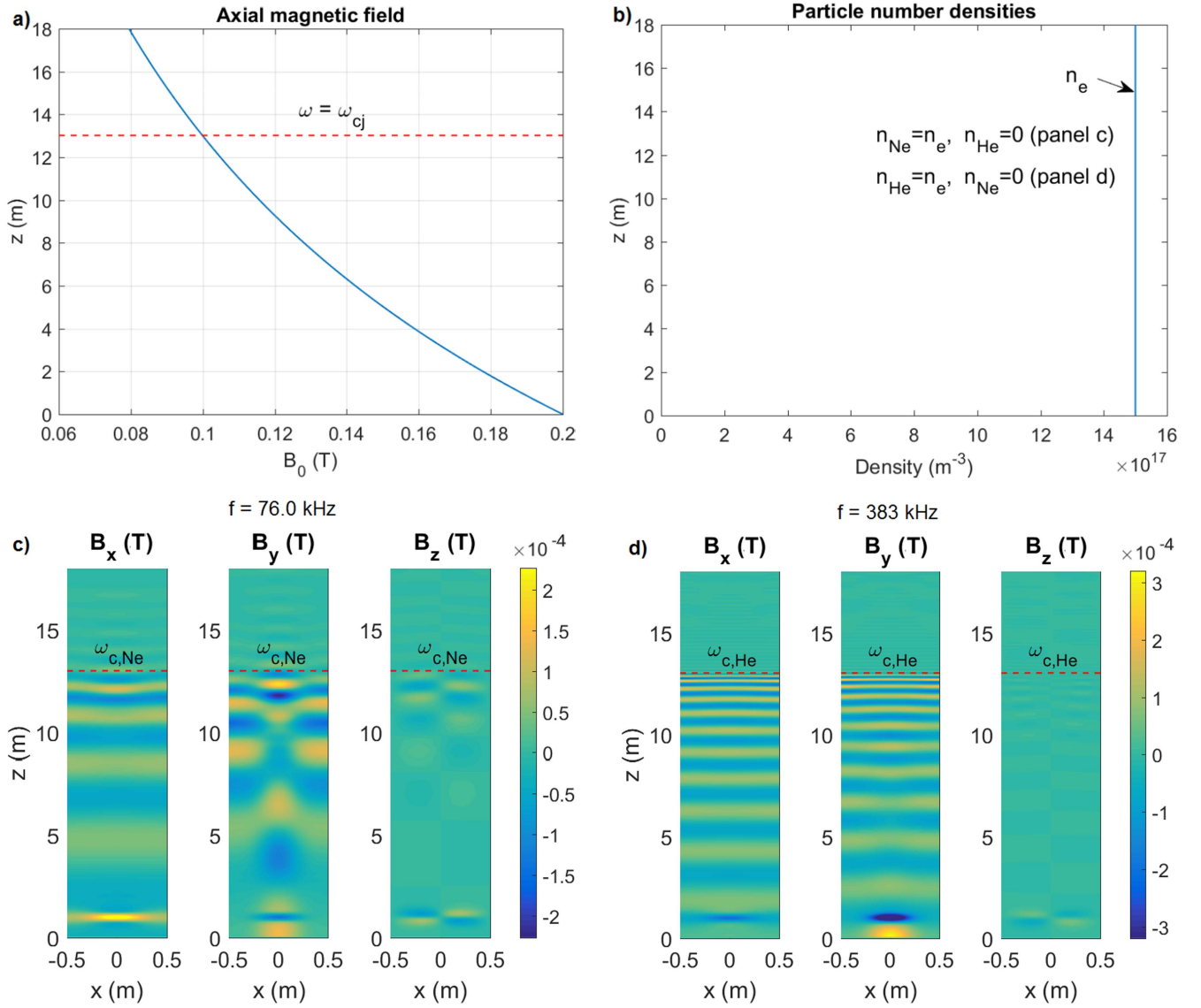
Figure 3. The propagation of EMIC waves in single ion Ne and He plasmas, showing (a) the axial magnetic field, (b) particle number densities, with $n_e = 1.5 \times 10^{18}$ m^{-3} and with $n_{Ne} = n_e$, $n_{He} = 0$ in panel (c) and $n_{He} = n_e$, $n_{Ne} = 0$ in panel (d). L-polarized EMIC waves are excited at $z = 1$ m, with frequency $\omega = 4.77 \times 10^5$ s^{-1} ($f = 76$ kHz) (panel (c)) and $\omega = 4.82 \times 10^6$ s^{-1} ($f = 383$ kHz) (panel (d)), which respective equal $\omega_{c,Ne}$ and $\omega_{c,He}$ at $z \approx 13$ m where $B = 0.1$ T (dashed horizontal lines). For clarity, the horizontal axes have been enhanced in panels (c) and (d).

resonance in figure 3(d) compared to the Ne resonance in figure 3(c).

In figure 4, the same magnetic field profile as in figure 3 is used, but with spatially varying ion number densities in a mixture of Ne and He ions and with a spatially increasing He number density along the z-axis. Ion cyclotron resonances occur at $z = 13$ m (same as in figure 3) for the transmitted frequencies $f = 76$ kHz and $f = 383$ kHz, and an ion–ion hybrid cutoff at $z \approx 4.3$ m (see figure 4(d)) for $f = 383$ kHz. In the latter case, the source at $z = 1$ m is within the evanescent region, and the EMIC waves must tunnel through the evanescent region to become propagating waves for 4.3 m $< z < 13$ m. It should be noted that while EMIC waves can tunnel through a small evanescent region in a

laboratory plasma, the effect would be more significant in the ionosphere due to much larger gradient length-scales.

4. Pitch angle diffusion of relativistic electrons

While the magnetic moment of a relativistic electron (e.g. Walt 1994, Öztürk 2016) $\mu = \gamma^2 m_e v_\perp^2/(2B)$ is nearly conserved in a slowly varying magnetic field, hydromagnetic waves can resonantly scatter and break the conservation of the magnetic moment, leading to an increased precipitation of mirror contained electrons. Here, $\gamma = 1/\sqrt{1 - v_0^2/c^2}$ is the relativistic gamma factor, v_0 is the speed of the electron, and $v_\perp$ is the magnitude of the velocity of the electron perpendicular to the
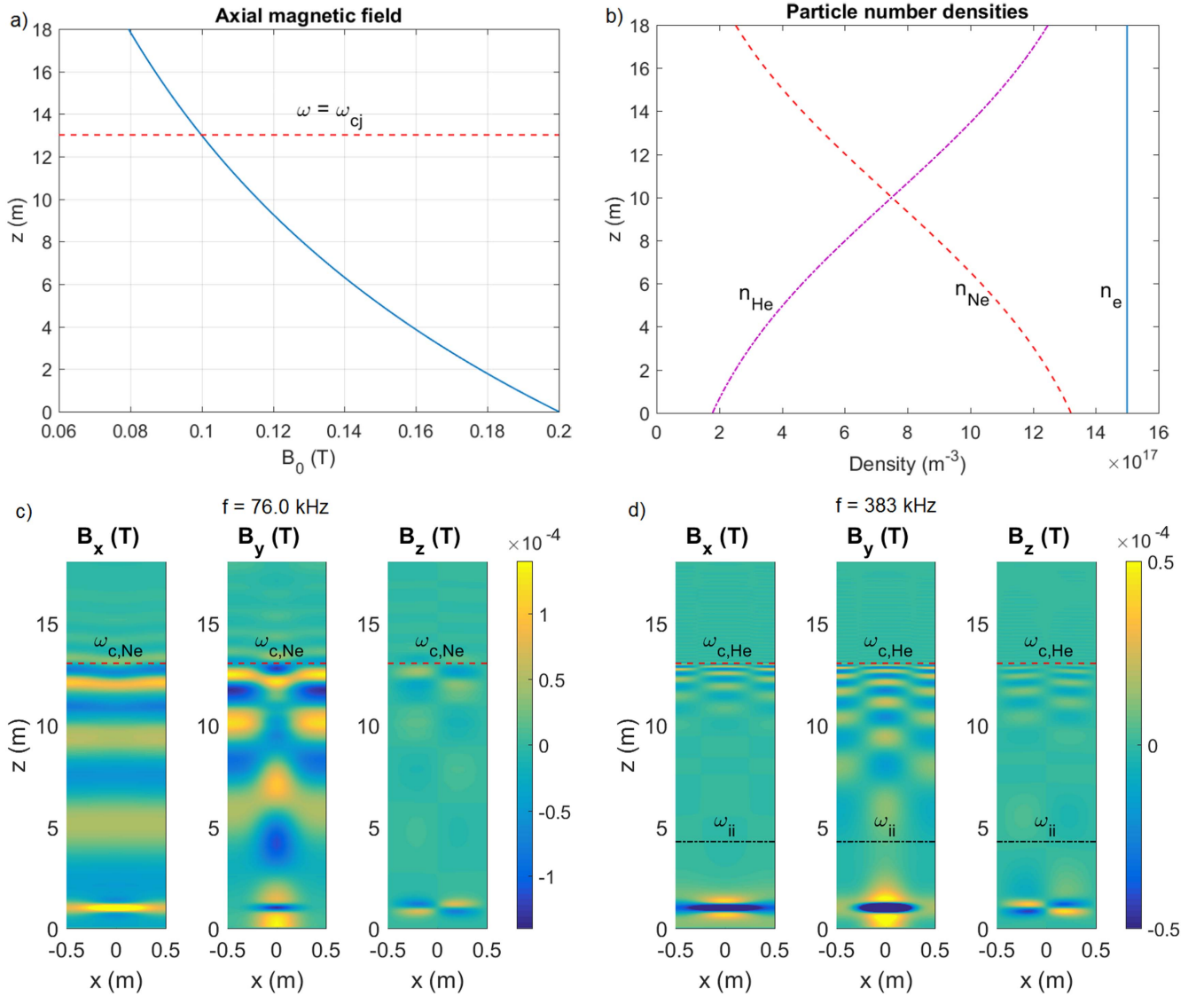
Figure 4. The propagation of EMIC waves in two-ion Ne-He plasma showing (a) the axial magnetic field, (b) particle number densities, with $n_e = 1.5 \times 10^{18}$ m^{-3} with spatially varying ion number densities keeping $n_{Ne} + n_{He} = n_e$. L-polarized EMIC waves are excited at $z = 1$ m, with frequencies $\omega = 4.77 \times 10^5$ s^{-1} ($f = 76$ kHz) (panel (c)) and $\omega = 4.82 \times 10^6$ s^{-1} ($f = 383$ kHz) (panel (d)) which respectively equal $\omega_{c,Ne}$ and $\omega_{c,He}$ at $z \approx 13$ m where $B = 0.1$ T (horizontal dashed lines). The ion–ion hybrid cutoff $\omega = \omega_{ii} = \sqrt{\left(\omega^2_{c,Ne}\omega^2_{p,He} + \omega^2_{c,He}\omega^2_{p,Ne}\right)/\left(\omega^2_{p,Ne} + \omega^2_{p,He}\right)}$ is at $z \approx 4.3$ m for $f = 383$ kHz (panel (d), dashed–dotted line). For clarity, the horizontal axes have been enhanced in panels (c) and (d).

magnetic field. Models exist for the pitch angle scattering of charged particles by broadband hydromagnetic waves in the Earth's dipole magnetic field (Lyons and Williams 1984, Summers and Thorne 2003, Shao *et al* 2009). The question is how efficiently the EMIC waves near cyclotron resonances pitch angle scatter relativistic electrons. The Doppler resonance condition between a relativistic electron and an EMIC wave propagating parallel to the magnetic field is (e.g. Summers and Thorne 2003) $\omega - v_\parallel k = -\omega_{ce}/\gamma$ where $v_\parallel = v_0 \cos\alpha$ is the parallel component of the electron's velocity and $\alpha = \arcsin(v_\perp/v_0)$ is the pitch angle. Omitting the ω-term, which is justified since $\omega \ll \omega_{ce}$ for EMIC waves, the resonance condition can be written

$$k = \frac{\omega_{ce}}{\gamma v_0 \cos\alpha}. \tag{19}$$

The spatially varying wave magnetic field (see figure 2) may interact resonantly with relativistic electrons where the EMIC wave locally fulfills the resonance condition (19). To derive a diffusion coefficient for the pitch angle scattering of relativistic electrons, we first calculate the spatial Fourier transform of the wave magnetic field (see appendix B),

$$\hat{B}(k) = \int_\infty^{-\infty} B(\xi)e^{-ik\xi}d\xi = \frac{iB_{01}}{k}$$

$$\times \begin{cases} -\left[1 + \frac{2}{\pi}\text{Si}\left(\frac{\kappa_j}{k}\right)\right]\cos\left(\frac{\kappa_j}{k}\right), \ k < 0 \\ 2\exp\left(-i\frac{\kappa_j}{k}\right) + \left[1 - \frac{2}{\pi}\text{Si}\left(\frac{\kappa_j}{k}\right)\right]\cos\left(\frac{\kappa_j}{k}\right), \ k > 0, \end{cases} \tag{20}$$

where $\mathrm{Si}(z) = \int_z^0 \frac{\sin t}{t} \mathrm{d}t$ is the sine integral (Abramowitz and Stegun 1964). It holds that that $\mathrm{Si}(z) \approx -\pi/2 - \cos(z)/z$ for $z \ll -1$, $\mathrm{Si}(z) \approx -\pi/2 - \cos(z)/z$ for $z \gg 1$, and $\mathrm{Si}(z) \approx z$ for $|z| \ll 1$. A good approximation of equation (20) for $|\kappa_j/k| > 1$ is therefore

$$\hat{B}(k) = \frac{\mathrm{i}B_{01}}{k} \begin{cases} 0, & k < 0 \\ 2\exp\left(-\mathrm{i}\frac{\kappa_j}{k}\right), & k > 0. \end{cases} \quad (21)$$

Hence, an EMIC wave which is monochromatic in time has a broadband spatial spectrum near the cyclotron resonance. The scattering of charged particles due to broadband electromagnetic waves can be treated with quasilinear theory (Melrose 1980, Steinacker and Miller 1992). Summers and Thorne (2003) give the pitch angle diffusion coefficient on the form

$$D_{\alpha\alpha} = \frac{\omega_{ce}}{\gamma} \frac{|k| \; \hat{W}(k)}{W_0}, \quad (22)$$

where $W_0 = B_0^2/2\mu_0$ is the background magnetic field energy density, and $\hat{W}(k)$ is the wave magnetic field spectral density normalized such that $W_{\mathrm{tot}} = \int \hat{W}(k)\mathrm{d}k$, where $W_{\mathrm{tot}} = B^2/2\mu_0$ is the spatially averaged wave magnetic energy density. Assuming a spatial average over a domain d much larger than the EMIC wavelength, we have the spectral density

$$\hat{W}(k) = \frac{|\hat{B}(k)|^2}{4\pi\mu_0 d}. \quad (23)$$

Using equation (23) in equation (22) then gives the pitch angle diffusion coefficient

$$D_{\alpha\alpha} = \frac{\omega_{ce}|k|}{2\pi\gamma d} \frac{|\hat{B}(k)|^2}{B_0^2}, \quad (24)$$

with $\hat{B}(k)$ given by equation (20). Using instead the approximate expression (21) in equation (24) gives

$$D_{\alpha\alpha} = \frac{2\omega_{ce}}{\pi\gamma|k|} \frac{|B_{01}|^2}{d} \frac{1}{B_0^2} = \frac{2v_0 \cos(\alpha)}{\pi d} \frac{|B_{01}|^2}{B_0^2}, \quad (25)$$

for $k > 0$ and $D_{\alpha\alpha} = 0$ for $k < 0$, and where the resonance condition (19) was used in the last step in equation (25). For multi-MeV electrons, we can use $v_0 \approx c$. The diffusion coefficient given in equations (24) and (25) are plotted in figure 5 as solid and dashed lines, respectively. It is seen that $D_{\alpha\alpha}$ to a good approximation grows linearly with positive κ_j/k and is negligibly small for negative κ_j/k. The asymmetry of the diffusion coefficient with respect to the sign of κ_j/k reflects that the L-polarized EMIC wave interacts resonantly with electrons propagating in the same direction as the wave, but not with electrons propagating in the opposite direction.

For mirror-contained electrons, we can estimate the effective domain length $d = v_z t_B = v_0 \cos(\alpha)t_B$, where t_B is the bounce period, which inserted into equation (25) gives the bounce-averaged pitch angle diffusion coefficient

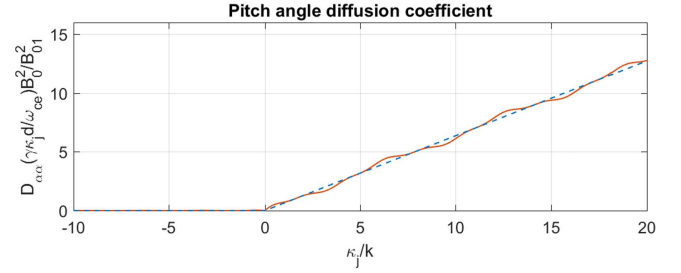$$\langle D_{\alpha\alpha} \rangle = \frac{2}{\pi t_B} \frac{|B_{01}|^2}{B_0^2}. \quad (26)$$

Figure 5. Normalized pitch angle diffusion coefficient $D_{\alpha\alpha}(\gamma\kappa_j d/\omega_{ce})B_0^2/B_{01}^2$ (solid line) as a function of κ_j/k, where $\kappa_j = \omega_{pj}^2 L/c^2$, and $k(\alpha)$ is given by equation (20) with α being the pitch angle. Efficient pitch angle diffusion occurs only for $\kappa_j/k > 0$, i.e. for electrons propagating in the same direction as the EMIC wave. The solid line is given by the expression (24) while the dashed line shows the approximation (25).

Using equation (26), the spread in pitch angle after time t may roughly be estimated as

$$\Delta\alpha = \sqrt{\langle D_{\alpha\alpha} t \rangle} = \frac{B_{01}}{B_0} \sqrt{\frac{2t}{\pi t_B}}. \quad (27)$$

It is desirable to express the diffusion coefficient (26) and pitch angle spread (27) in terms of the local wave magnetic field amplitude $|B|$ where the resonant wave-particle interaction takes place. Using large argument expansions of the Bessel functions J_0 and Y_0 in equation (16) gives $|B| \approx B_{01}/(\sqrt{\pi} \; |\kappa_j\xi|^{1/4})$ for $2|\kappa_j\xi|^{1/2} \gg 1$. The phase of the EMIC wave varies approximately as $\theta = 2|\kappa_j\xi|^{1/2}$, and hence the local wavenumber can be taken as $k' = \partial\theta/\partial\xi = |\kappa_j/\xi|^{1/2}$. Resonant wave-particle interaction takes place where $k' = k$, i.e. where $|\kappa_j\xi| = \kappa_j^2/k^2$. This gives $|B| \approx B_{01}/(\pi\kappa_j/k)^{1/2}$; solving for B_{01} and inserting the result into equations (26) and (27) gives

$$\langle D_{\alpha\alpha} \rangle = \frac{2}{t_B} \frac{\kappa_j}{k} \frac{|B|^2}{B_0^2} \quad (28)$$

and

$$\Delta\alpha = \frac{|B|}{B_0} \sqrt{2\frac{\kappa_j}{k}\frac{t}{t_B}}, \quad (29)$$

respectively, where $|B|$ is evaluated in space at $|\xi| = \kappa_j/k^2$.

As an application of the above results we consider injecting 2 MeV electrons ($\gamma \approx 5$, $v_0 \approx c$) with a pitch angle of $\alpha = \pi/4$, giving the parallel velocity $v_\parallel \approx 0.7c$ in the UCLA LAPD chamber under the conditions discussed previously (see figures 3 and 4). The results are summarized in table 1. The high-energy electrons with large pitch angles could for example be injected via electron cyclotron resonance heating (ECRH), in a similar manner as was done by Wang *et al* (2012, 2014). To mirror contain these electrons, the magnetic field should be significantly increased near both ends (both the high-field and low-field) of the device to form 'magnetic plugs' (not shown in figures 3 and 4). The condition for containment is $R_M > 1/\sin^2(\alpha)$ for the mirror ratio $R_M = B_{\max}/B_0$. For a magnetic field of $B_0 = 0.1$ T near the EMIC resonance layer (see figure 3), it is thus required that $B_{\max} > 2B_0 = 0.2$ T to mirror contain an electron with pitch

Table 1. The pitch angle scattering of relativistic electrons by EMIC waves with parameters for Ne and He laboratory plasma (see figure 3) relevant to the UCLA LAPD chamber. For 2 MeV electrons having the initial pitch angle $\alpha = \pi/4$, and EMIC waves of amplitude 1% of the background magnetic field, the typical lifetime is of the order 1 ms or less.

Species	B_0	$|B|/B_0$	k (m^{-1})	κ_j (m^{-1})	t_B (s)	$\langle D_{\alpha\alpha} \rangle$ (s^{-1})	t_{life} (ms)
Ne	0.1	0.01	16	30	1.7×10^{-7}	2.25×10^3	1
He	0.1	0.01	16	153	1.7×10^{-7}	1.2×10^4	0.2

angle $\alpha = \pi/4$. The non-relativistic electron cyclotron frequency is $\omega_{ce} \approx 1.8 \times 10^{10}$ s^{-1}, and the condition (19) gives a resonant wavenumber $k = 16$ m^{-1}. For mirror contained electrons in the UCLA LAPD device (axial length ~ 18 m), the bounce time back and forth once in the mirror field would be $t_B \approx 2 \times 18/(0.7\,c) = 1.7 \times 10^{-7}$ s. Using the parameters in figure 3, with $\kappa_{\text{Ne}} = 30$ m^{-1} and $\kappa_{\text{He}} = 153$ m^{-1}, gives $\kappa_{\text{Ne}}/k = 1.9$ and $\kappa_{\text{He}}/k = 10$ and assuming a large wave amplitude such that $|B|/B_0 = 0.01$ (e.g. Carter *et al* 2006, Auerbach *et al* 2010, Howes *et al* 2012, Dorfman and Carter 2013, 2015, 2016) would give (see equation (28)) $\langle D_{\alpha\alpha} \rangle \approx 2.25 \times 10^3$ s^{-1} for the Ne case and $\langle D_{\alpha\alpha} \rangle \approx 1.2 \times 10^4$ s^{-1} for the He case. After $t = 10^{-6}$ s (about 5 bounces back and forth) the pitch angle spread (equation (29)) would be $\Delta\alpha \approx 0.05$ rad for the Ne case and $\Delta\alpha \approx 0.1$ rad for the He case. The typical lifetime of a relativistic electron depends on the mirror ratio of the experiment, the initial distribution of the electrons, etc. As a crude estimate, it can be assumed that the electrons have a significant probability to being scattered into the loss cone when the $\Delta\alpha \approx \pi/2$ rad. Using $\Delta\alpha \approx \pi/2$ in equation (29) and solving for time, the estimated lifetime is

$$t_{\text{life}} = \frac{\pi^2}{8} \frac{k}{\kappa_j} \frac{B_0^2}{|B|^2} t_B. \tag{30}$$

This gives the lifetime $t_{\text{life}} = 1$ ms for the Ne case and $t_{\text{life}} = 0.2$ ms for the He case. It should be noted from equation (30) that the lifetime scales as the inverse square of the wave amplitude, and from the definition $\kappa_j = \omega_{pj}^2 L/c^2$ (see equation (14)) the lifetime is inversely proportional to the length-scale L of the magnetic field at the ion cyclotron resonance, i.e. larger L leads to more efficient electron scattering. The locations of the strongest resonant electron-wave interaction is $|\xi| = \kappa_{\text{Ne}}/k^2 \approx 0.13$ m for the Ne case and $|\xi| = \kappa_{\text{Ne}}/k^2 \approx 0.63$ m for the He case. Hence, the resonant interaction occurs at $z \approx 13 - 0.13 = 12.87$ m for the Ne case (see figure 3(c)), and $z \approx 13 - 0.63 = 12.37$ m for the He case (see figure 3(d)). Both cases fit well in an experiment.

It is interesting that Wang *et al* (2012, 2014) in their experiment observed efficient scattering of electrons by *right-hand* polarized Alfvén/whistler waves, which they attributed to the interference between the whistler wave and the electron's azimuthal grad-B drift motion also occurring in the right-hand direction, but no efficient electron scattering by left-hand polarized EMIC waves. However, their launched EMIC wave frequency was significantly lower than the ion cyclotron frequency, resulting in a wavelength too long to resonantly pitch angle scatter the electrons.

The ultimate goal is to model electron scattering by EMIC waves in the ionosphere. As an example of parameters of the Earth's ionosphere at an altitude of 2000 km, we take the magnetic field $B_0 = 1.3 \times 10^{-5}$ T giving the electron cyclotron frequency $\omega_{ce} \approx 2.3 \times 10^6$ s^{-1}, and the number density of hydrogen ions $n_H \sim 10^{10}$ m^{-3} corresponding to the hydrogen plasma frequency $\omega_{pH} = 1.3 \times 10^5$ s^{-1}. We again consider 2 MeV electrons, with $\gamma = 5$ and $v_0 \approx c$. Using a typical local magnetic field length-scale $L \sim 1.5 \times 10^6$ m would give $\kappa_H = \omega_{pH}^2 L/c^2 = 0.3$ m^{-1}, while the resonance condition (19) gives the resonant wavenumber $k = 2.2 \times 10^{-3}$ m^{-1} so that $\kappa_H/k = 136$. A typical relativistic electron at an altitude of 2000 km near the equator has a bounce period of the order $t_B \approx 0.1$ s (e.g. Hess 1962). Taking the EMIC wave magnetic field $B = 10^{-9}$ T gives (see equation (28)) $\langle D_{\alpha\alpha} \rangle \approx 3.2 \times 10^{-5}$ s^{-1} and (see equation (29)) $\Delta\alpha = 5.7 \times 10^{-3}\sqrt{t}$ (with t in seconds). The typical lifetime of an electron can be taken as when it has been pitch angle deflected to $\Delta\alpha \approx \pi/2$ rad, which is reached when $t \approx 6 \times 10^4$ s (~ 16 h). Taking into account a similar degree of pitch angle scattering at the conjugate hemisphere would decrease the lifetime a factor two to 3×10^4 s (~ 8 h). The resonant interaction between the electrons and EMIC wave would take place at a distance $|\xi| = 4\kappa_j/k^2 \approx 250$ km away from the EMIC resonance layer. There will also be a longitudinal grad-B drift of the electrons with a revolution of the order of an hour. If the EMIC waves are present only in localized regions, the drift-averaged diffusion coefficient may be a few orders of magnitude smaller than $\langle D_{\alpha\alpha} \rangle$ and the lifetime correspondingly longer (e.g. Summers and Thorne 2003).

5. Conclusions

The propagation of EMIC waves near the cyclotron resonances and the pitch angle scattering of relativistic electrons have been studied theoretically. Multi-ion plasma introduce cyclotron resonances at locations where the wave frequency matches the respective ion cyclotron frequency, and in addition ion–ion hybrid cutoffs where the wave frequency matches the ion–ion resonance frequency. Due to the inhomogeneous magnetic field and rapidly spatially changing wavelength near a cyclotron resonance, a monochromatic (in time) EMIC wave gives rise to a broadband spectrum of waves in space, where relativistic electrons are resonantly pitch angle scattered by the EMIC wave when the local wavenumber fulfills the electron cyclotron resonance

condition. Simple expressions for the pitch angle diffusion coefficient are derived using the spatial profile (Stix 1960, 1992) of the wave magnetic field near an ion cyclotron resonance. The theory is relevant to laboratory plasmas such as the UCLA LAPD experiment, where a typical lifetime for a mirror-contained relativistic electron is predicted to be of the order of a millisecond using an EMIC wave magnetic field of the order 1% of the ambient magnetic field. Ultimately the application of the theory is to mirror contained electrons in the Earth's ionosphere, where EMIC waves can pitch angle scatter energetic electrons near the EMIC resonance regions.

Acknowledgments

Appendix A. Numerical multi-ion model

A collisional Hall-MHD model was developed by Eliasson *et al* (2012) (see also Sharma *et al* (2016) for polar coordinates), where plasma conductivities and dielectric constants were derived from the electron and ion momentum equations. We here slightly modify the formulation of Eliasson *et al* (2012) to include multiple ion species. Introducing the vector and scalar potentials $\mathbf{A}$ and ϕ through $\mathbf{B} = \nabla \times \mathbf{A}$ and $\mathbf{E} = -\nabla \phi - \partial \mathbf{A}/\partial t$ with the Weyl (or temporal) gauge $\phi = 0$, we have

$$\frac{\partial \mathbf{A}}{\partial t} = -\mathbf{E}, \qquad (A1)$$

which effectively replaces Faraday's law. For two-ion species, we have the momentum equations

$$\frac{\partial \mathbf{v}_{i1}}{\partial t} = \frac{e}{m_{i1}}(\mathbf{E} + B_0 \overline{\overline{\mathbf{R}}}_{i1}\mathbf{v}_{i1}) \qquad (A2)$$

and

$$\frac{\partial \mathbf{v}_{i2}}{\partial t} = \frac{e}{m_{i2}}(\mathbf{E} + B_0 \overline{\overline{\mathbf{R}}}_{i2}\mathbf{v}_{i2}), \qquad (A3)$$

where we denoted $\overline{\overline{\mathbf{R}}}_{i1}\mathbf{v}_{i1} \equiv \mathbf{v}_{i1} \times \mathbf{B}_0/B_0 - m_{i1}\nu_{i1}\mathbf{v}_{i1}/eB_0$ and $\overline{\overline{\mathbf{R}}}_{i2}\mathbf{v}_{i2} \equiv \mathbf{v}_{i2} \times \mathbf{B}_0/B_0 - m_{i2}\nu_{i2}\mathbf{v}_{i2}/eB_0$, and ν_{i1} and ν_{i1} are ion-neutral collision frequencies. The electric field is given by the electron momentum equation with inertialess electrons,

$$\mathbf{E} = -B_0 \overline{\overline{\mathbf{R}}}_e \mathbf{v}_e, \qquad (A4)$$

where we denoted $\overline{\overline{\mathbf{R}}}_e \mathbf{v}_e \equiv \mathbf{v}_e \times \mathbf{B}_0/B_0 + m_e\nu_e\mathbf{v}_e/eB_0$, and ν_e is the electron-neutral collision frequency. The electron

velocity is obtained from Ampère's law as

$$\mathbf{v}_e = \frac{1}{n_e}(n_{i1}\mathbf{v}_{i1} + n_{i2}\mathbf{v}_{i2}) - \frac{\nabla \times (\nabla \times \mathbf{A})}{\mu_0 e n_e} + \frac{\mathbf{j}_{ext}}{e n_e}, \qquad (A5)$$

together with the quasineutrality condition $n_e = n_{i1} + n_{i2}$. The displacement current has been neglected in equation (15) with the assumption that the wave speed is much smaller than the speed of light. In the numerical examples, collisions are neglected, hence $\nu_{i1} = \nu_{i2} = \nu_e = 0$.

The external current source $\mathbf{j}_{ext}$ is employed to inject circularly polarized waves into the plasma by a left-hand rotating current source. We use the divergence-free external current source

$$\mathbf{j}_{ext} = j_0 \frac{\hat{\mathbf{x}}z \cos(\omega t) + \hat{\mathbf{y}}z \sin(\omega t) - \hat{\mathbf{z}}x \cos(\omega t)}{a}$$
$$\times \sqrt{2}\, e^{1/2} e^{-(x^2 + (z - z\_0)^2)/a^2}, \qquad (A6)$$

where j_0 the peak amplitude of the current density, and a and z_0 is the width and axial position of the source. We use $j_0 = 2$ kA m^{-2}, $a = 0.2$ m and $z_0 = 1$ m in the simulations. Equations (A1)–(A6) are solved numerically, using a simulation box with dimensions——-0.5 m $\leqslant x \leqslant 0.5$ m and $0 \leqslant z \leqslant 18$ m, which is close to the dimensions of the UCLA LAPD chamber. The simulation domain is resolved on a uniform numerical grid with 20 intervals in the x-direction and 400 intervals in the y-direction. For simplicity, periodic boundary conditions are used in the x-direction while reflecting boundaries $A_x = A_y = 0$ and $\partial A_z/\partial z = 0$ are used at $z = 0$ and $z = 18$ m. Spatial derivatives with respect to x are calculated using a pseudo-spectral method while z-derivatives are approximated by centered 2nd-order difference approximations. A standard 4th order Runge–Kutta scheme is used to advance the solution in time, with a time-step of 10^{-9} s. It should be noted that equation (13) can be derived from equations (A1)–(A5) using $\mathbf{j}_{ext} = 0$ and the assumption that all time-dependent quantities are proportional to $\exp(-i\omega t)$.

Appendix B. Integral relations for the Fourier transform of the magnetic field

In calculating the Fourier transform (21) of the magnetic field in (17), use were made of the following integral relations for $k > 0$ (and $\kappa_j > 0$):

$$\int_{-\infty}^{0} J_0(2\sqrt{-\kappa_j \xi})\cos(k\xi)\,\mathrm{d}\xi = \frac{1}{k}\sin\left(\frac{\kappa_j}{k}\right), \qquad (B1)$$

$$\int_{-\infty}^{0} J_0(2\sqrt{-\kappa_j \xi})\sin(k\xi)\,\mathrm{d}\xi = -\frac{1}{k}\cos\left(\frac{\kappa_j}{k}\right), \qquad (B2)$$

$$\int_{-\infty}^{0} Y_0(2\sqrt{-\kappa_j \xi})\cos(k\xi)\,\mathrm{d}\xi = \frac{1}{\pi k}\left[\left(\mathrm{Si}\left(\frac{\kappa_j}{k}\right)\right)\left(-\frac{3\pi}{2}\right)\cos\right.$$
$$\left. \times \left(\frac{\kappa_j}{k}\right) + \mathrm{Ci}\left(\frac{\kappa_j}{k}\right)\sin\left(\frac{\kappa_j}{k}\right)\right], \qquad (B3)$$

$$\int_{-\infty}^{0} Y_0(2\sqrt{-\kappa_j \xi})\sin(k\xi)\mathrm{d}\xi = -\frac{1}{\pi k}\left[\mathrm{Si}\left(\left(\frac{\kappa_j}{k}\right)+\frac{\pi}{2}\right)\sin\right.$$
$$\left.\times\left(\frac{\kappa_j}{k}\right)+\mathrm{Ci}\left(\frac{\kappa_j}{k}\right)\cos\left(\frac{\kappa_j}{k}\right)\right],$$
$$(B4)$$

$$\int_{0}^{\infty} K_0(2\sqrt{\kappa_j \xi})\cos(k\xi)\mathrm{d}\xi = \frac{1}{2k}\left[-\left(\mathrm{Si}\left(\frac{\kappa_j}{k}\right)-\frac{\pi}{2}\right)\cos\right.$$
$$\left.\times\left(\frac{\kappa_j}{k}\right)+\mathrm{Ci}\left(\frac{\kappa_j}{k}\right)\sin\left(\frac{\kappa_j}{k}\right)\right],$$
$$(B5)$$

$$\int_{0}^{\infty} K_0(2\sqrt{\kappa_j \xi})\sin(k\xi)\mathrm{d}\xi = -\frac{1}{2k}\left[\left(\mathrm{Si}\left(\frac{\kappa_j}{k}\right)-\frac{\pi}{2}\right)\sin\right.$$
$$\left.\times\left(\frac{\kappa_j}{k}\right)+\mathrm{Ci}\left(\frac{\kappa_j}{k}\right)\cos\left(\frac{\kappa_j}{k}\right)\right],$$
$$(B6)$$

where $\mathrm{Ci}(x)$ is the cosine integral of argument x (Abramowitz and Stegun 1964). For $k < 0$, a temporary substitution $k = -k'$ with $k' > 0$ was made to evaluate the integrals, followed by a back-substitution $k' = -k$.

References

Abramowitz M and Stegun I A 1964 *Handbook of Mathematical Functions with Formulas, Graphs, and Mathematical Tables* (Washington DC: United States Department of Commerce, National Bureau of Standards) ch 5, p 231

Auerbach D W, Carter T A, Vincena S and Popovich P 2010 Control of gradient-driven instabilities using shear Alfvén beat waves *Phys. Rev. Lett.* **105** 135005

Carter T A, Brugman B, Pribyl P and Lybarger W 2006 Laboratory observation of a nonlinear interaction between shear Alfvén waves *Phys. Rev. Lett.* **96** 155001

Dorfman S and Carter T A 2013 Nonlinear excitation of acoustic modes by large-amplitude Alfvén waves in a laboratory plasma *Phys. Rev. Lett.* **110** 195001

Dorfman S and Carter T A 2015 Non-linear Alfvén wave interaction leading to resonant excitation of an acoustic mode in the laboratory *Phys. Plasmas* **22** 055706

Dorfman S and Carter T A 2016 Observation of an Alfvén wave parametric instability in a laboratory plasma *Phys. Rev. Lett.* **110** 195001

Eliasson B, Chang C-L and Papadopoulos K 2012 Generation of ELF and ULF electromagnetic waves by modulated heating of the ionospheric F2 region *J. Geophys. Res. Space Phys.* **117** A10320

Engebretson M J *et al* 2015 Van Allen probes, NOAA, GOES, and ground observations of an intense EMIC wave event extending over 12 h in magnetic local time *J. Geophys. Res. Space Phys.* **120** 5465–88

Farmer W A and Morales G J 2013 Propagation of shear Alfvén waves in two-ion species plasmas confined by a nonuniform magnetic field *Phys. Plasmas* **20** 082132

Hess W N 1962 Energetic particles in the inner Van Allen belt *Space Sci. Rev.* **1** 278–312

Howes G G, Drake D J, Nielson K D, Carter T A, Kletzing C A and Skiff F 2012 *Phys. Rev. Lett.* **109** 255001

Kubota Y, Omura Y and Summers D 2015 Relativistic electron precipitation induced by EMIC-triggered emissions in a dipole magnetosphere *J. Geophys. Res. Space Phys.* **120** 4384–99

Lyons L and Williams D 1984 Quantitative Aspects of Magnetospheric Physics *Geophysics and Astrophysics Monographs* (Dordrecht: Reidel Publishing Co.)

Melrose D B 1980 *Plasma Astrophysics, Nonthermal Processes in Diffuse Magnetized Plasmas* vol II (Newark, NJ: Gordon and Breach)

Morley S K, Friedel R H W and Noveroske E 2010 A rapid, global and prolonged electron radiation belt dropout observed with the Global Positioning System constellation *Geophys. Res. Lett.* **37** L06102

Omura Y, Pickett J, Grison B, Santolik O, Dandouras I, Engebretson M, Décréau P M E and Masson A 2010 Theory and observation of electromagnetic ion cyclotron triggered emissions in the magnetosphere *J. Geophys. Res.* **115** A07234

Öztürk M K 2016 Trajectories of charged particles trapped in Earth's magnetic field *Am. J. Phys.* **80** 420–8

Perkins F W 1977 Heating tokamaks via the ion-cyclotron and ion–ion hybrid resonances *Nucl. Fusion* **17** 1197–224

Roberts D R and Hershkowitz N 1992 Enhanced slow-wave beach heating of mirror plasmas with two-ion species *Phys. Fluids* B **4** 1475–85

Shao X, Papadopoulos K and Sharma A S 2009 Control of the energetic proton flux in the inner radiation belt by artificial means *J. Geophys. Res.* **114** A07214

Sharma A S, Eliasson B, Shao X and Papadopoulos K 2016 Generation of ELF waves during HF heating of the ionosphere at midlatitudes *Radio Sci.* **51** 962–71

Steinacker J and Miller J A 1992 Stochastic gyroresonant electron acceleration in a low-beta plasma: I. Interaction with parallel transverse cold plasma waves *Astrophys. J.* **393** 764–81

Stix T H 1958 Generation and thermalization of plasma waves *Phys. Fluids* **1** 308–17

Stix T H 1960 Absorption of plasma waves *Phys. Fluids* **3** 19–32

Stix T H 1992 *Waves in Plasmas* (New York: AIP) ch 13

Stix T H and Palladino R W 1958 Ion cyclotron resonance *Proc. 2nd UN Int. Conf. on the Peaceful Uses of Atomic Energy* vol 31 (Geneva: IAEA) pp 282–7

Summers D, Ni B and Meredith N P 2007 Timescales for radiation belt electron acceleration and loss due to resonant wave-particle interactions: II. Evaluation for VLF chorus, ELF hiss, and electromagnetic ion cyclotron waves *J. Geophys. Res.* **112** A04207

Summers D and Thorne R M 2003 Relativistic electron pitch-angle scattering by electromagnetic ion cyclotron waves during geomagnetic storms *J. Geophys. Res.* **108** 1143

Van Compernolle B, Bortnik J, Pribyl P, Gekelman W, Nakamoto M, Tao X and Thorne R M 2014 Direct detection of resonant electron pitch angle scattering by whistler waves in a laboratory plasma *Phys. Rev. Lett.* **112** 145006

Vincena S, Gekelman W and Maggs J 2001 Shear Alfvén waves in a magnetic beach and the roles of electron and ion damping *Phys. Plasmas* **8** 3884–96

Vincena S T, Farmer W A, Maggs J E and Morales G J 2011 Laboratory realization of an ion–ion hybrid Alfvén wave resonator *Geophys. Res. Lett.* **38** L11101

Vincena S T, Farmer W A, Maggs J E and Morales G J 2013 Investigation of an ion–ion hybrid Alfvén wave resonator *Phys. Plasmas* **20** 012111

Vincena S T, Morales G J and Maggs J E 2010 Effect of two ion species on the propagation of shear Alfvén waves of small transverse scale *Phys. Plasmas* **17** 052106

Walt M 1994 *Introduction to Geomagnetically Trapped Radiation* (*Cambridge Atmospheric and Space Science Series*) (New York: Cambridge University Press)

Wang Y, Gekelman W, Pribyl P and Papadopoulos K 2012 Scattering of magnetic mirror trapped fast electrons by a shear Alfvén wave *Phys. Rev. Lett.* **108** 105002

Wang Y, Gekelman W, Pribyl P and Papadopoulos K 2014 Enhanced loss of magnetic-mirror-trapped fast electrons by a shear Alfvén wave *Phys. Plasmas* **21** 055705